TRENDS IN SCIENCES 2026; 23(4): 12110
https://doi.org/10.48048/tis.2026.12110 RESEARCH ARTICLE

# New Synthetic Routes, Wound Healing and Hemostatic Properties of *N*-Guanidinium Chitosan

**Oliy Akhmedov[1,*], Jamoliddin Abdurakhmanov[1], Shavkat Shomurotov[1], Lijun You[2], Abbaskhan Turaev[1], Jaloliddin Makhkamov[1], Otabek Radjabov[1] and Arslon Khusenov[3]**

[1]*Institute of Bioorganic Chemistry of the Academy of Sciences of Uzbekistan, Tashkent 100125, Uzbekistan*
[2]*School of Food Science and Engineering, South China University of Technology, Guangzhou 510640, China*
[3]*Tashkent Institute of Chemical Technology, Tashkent 100011, Uzbekistan*

**([*]Corresponding author's e-mail: akhmedov.oliy@gmail.com)**

*Received: 29 September 2025, Revised: 13 October 2025, Accepted: 23 October 2025, Published: 25 December 2025*

**Abstract**

The development of novel multifunctional biomaterials remains one of the most pressing challenges in modern materials science. Polymer derivatives of guanidine are in high demand due to their broad spectrum of pharmacological activities. In recent years, various methods have been developed to introduce guanidine groups into the chitosan structure. However, most of the known guanidination methods are carried out in the presence of acids, which leads to the formation of side reactions in the reaction medium. In this study, we present a method for guanidination of chitosan in an aprotic solvent medium - acetonitrile. It has been demonstrated that by varying the molar ratio of the guanidinating reagent, it is possible to obtain *N*-guanidinium chitosan derivatives with a degree of substitution ranging from 0.16 to 0.45. Notably, the use of acetonitrile prevents hydrolysis of the chitosan macromolecular backbone, and an increase in the number of guanidine groups leads to an increase in the molecular weight of the synthesized *N*-guanidinium chitosan derivatives. The structure and properties of the obtained chitosan derivatives were confirmed by physico-chemical methods (elemental analysis, FTIR, NMR, XRD, SEM, DLS, etc.). The presence of guanidine groups in the chitosan structure conferred broad pH-range solubility to the synthesized compounds. Results from a comparative *in vivo* analysis demonstrated that 0.5% solutions of *N*-guanidinium chitosan exhibited excellent wound healing properties, attributed to the synergistic interaction between the polysaccharide backbone and the guanidine moieties. Pharmacological evaluations confirmed that the introduction of guanidine groups into the chitosan structure enhances its hemostatic efficacy compared to native chitosan.

**Keywords:** Chitosan, Modification, Guanidine, Acetonitrile, *N*-guanidinium chitosan, Wound healing, Hemostatic properties

## Introduction

In recent years, there has been a steady increase in interest toward the development of biocompatible and biodegradable materials with therapeutic properties. Particular attention is given to naturally derived polysaccharides as promising platforms for the rational design of novel biologically active polymeric materials [1,2]. Among various polysaccharides, chitosan is widely employed in the development of antimicrobial, wound-healing, hemostatic materials, and drug delivery systems due to its biocompatibility, structural features, unique physico-chemical properties, and inherent physiological activity [3-6]. Despite these advantages, chitosan possesses certain limitations that restrict its application in the design of bioactive polymers capable of dissolving in neutral or mildly alkaline physiological environments. Therefore, improving its solubility and expanding the spectrum of its biological activities remain fundamentally important challenges. Chemical modification remains the most rational approach to improving chitosan solubility by introducing new

functional groups into its structure. For example, the introduction of carboxymethyl functional groups into the monomeric units of chitosan significantly enhances its solubility. Carboxymethylation is typically carried out either at the amino groups (N-substitution) or at the hydroxyl groups (O-substitution), leading to the formation of carboxymethyl chitosan [7,8]. However, the incorporation of chemically bound anionic groups, while improving chitosan's solubility, results in a reduction of the original positive charge along the macromolecular backbone and consequently contributes to the partial or complete loss of its native properties [9,10]. This type of modification disrupts the delicate balance between hydrophilicity and cationic activity of the polymer. As a result, the decreased density of positive charges limits the ability of carboxymethyl chitosan to engage in electrostatic interactions with negatively charged biological components. This, in turn, leads to a noticeable attenuation of the intrinsic bioactivity of the parent chitosan.

In order to expand the functional potential and enhance the solubility of chitosan across a broad pH range, increasing attention has been directed toward the quaternization of amino groups [11,12]. This chemical modification introduces permanent quaternary ammonium moieties into the polymer backbone, thereby altering its charge distribution and imparting novel physicochemical properties. The incorporation of stable quaternary ammonium groups significantly improves chitosan's water solubility and markedly enhances its antimicrobial activity due to an increased density of positive charge. The presence of a permanent cationic charge along the polymer chain renders these derivatives particularly attractive for the development of multifunctional biomedical materials, including wound dressings, biodegradable films, and controlled drug delivery systems. However, despite these clear advantages, quaternized chitosan derivatives exhibit certain limitations, such as reduced biodegradability and potential cytotoxicity, which may hinder their practical application.

Guanidine as a functional moiety is characterized by low toxicity, high chemical stability, and a pronounced affinity for negatively charged components of cellular membranes, rendering it particularly promising for the development of biomedical polymeric materials [13-15]. Guanidine groups can maintain a protonated state across a broad pH range, thereby imparting enhanced biological activity to the synthesized cationic polymers. The reactive amino functionalities of guanidine enable interactions with various functional groups, including amino, carboxyl, and aldehyde moieties, thus broadening the scope of potential chemical modifications [16-18]. Collectively, these properties make guanidine a valuable building block for the design of novel compounds soluble under neutral and alkaline physiological conditions. Given that guanidine is a safe and reactive chemical agent exhibiting basic properties, its covalent incorporation into the chitosan backbone can not only significantly improve the polymer's solubility at elevated pH values but also enhance its therapeutic performance.

One of the reagents commonly used for the introduction of guanidine fragments into the chitosan backbone is cyanamide. Several studies have demonstrated the feasibility of its application for the guanidinylation of chitosan in the presence of aqueous acid solutions, which act both as solvents and as catalysts for the reaction [19,20]. However, despite the potential viability of this synthetic approach, its implementation is associated with a number of significant limitations, primarily related to the instability of cyanamide in acidic media. Under protonic conditions, cyanamide is prone to hydrolytic decomposition, leading to the formation of undesirable by-products and a marked decrease in the efficiency of guanidine group transfer to the polymer chain (**Figure 1(a)**). As a result, the reaction may proceed non-selectively, yielding side products and lowering the degree of functionalization of the chitosan matrix. An additional factor limiting the use of acidic solutions is the susceptibility of chitosan macromolecules to acid-catalyzed hydrolysis, which leads to polymer chain scission and a significant reduction in molecular weight (**Figure 1(b)**). This degradation process becomes particularly pronounced at elevated temperatures, necessitating the development of reaction conditions that minimize destructive side reactions. From a chemical standpoint, the guanidination of chitosan in the presence of aprotic solvents is of considerable interest due to its potential to enhance the efficiency of functional group modification. The use of aprotic solvents, particularly acetonitrile, can significantly increase the reactivity of the primary amino groups of

chitosan by preventing their protonation. Moreover, the application of aprotic media helps to minimize side reactions such as the decomposition of cyanamide or the hydrolysis of the chitosan macromolecule.

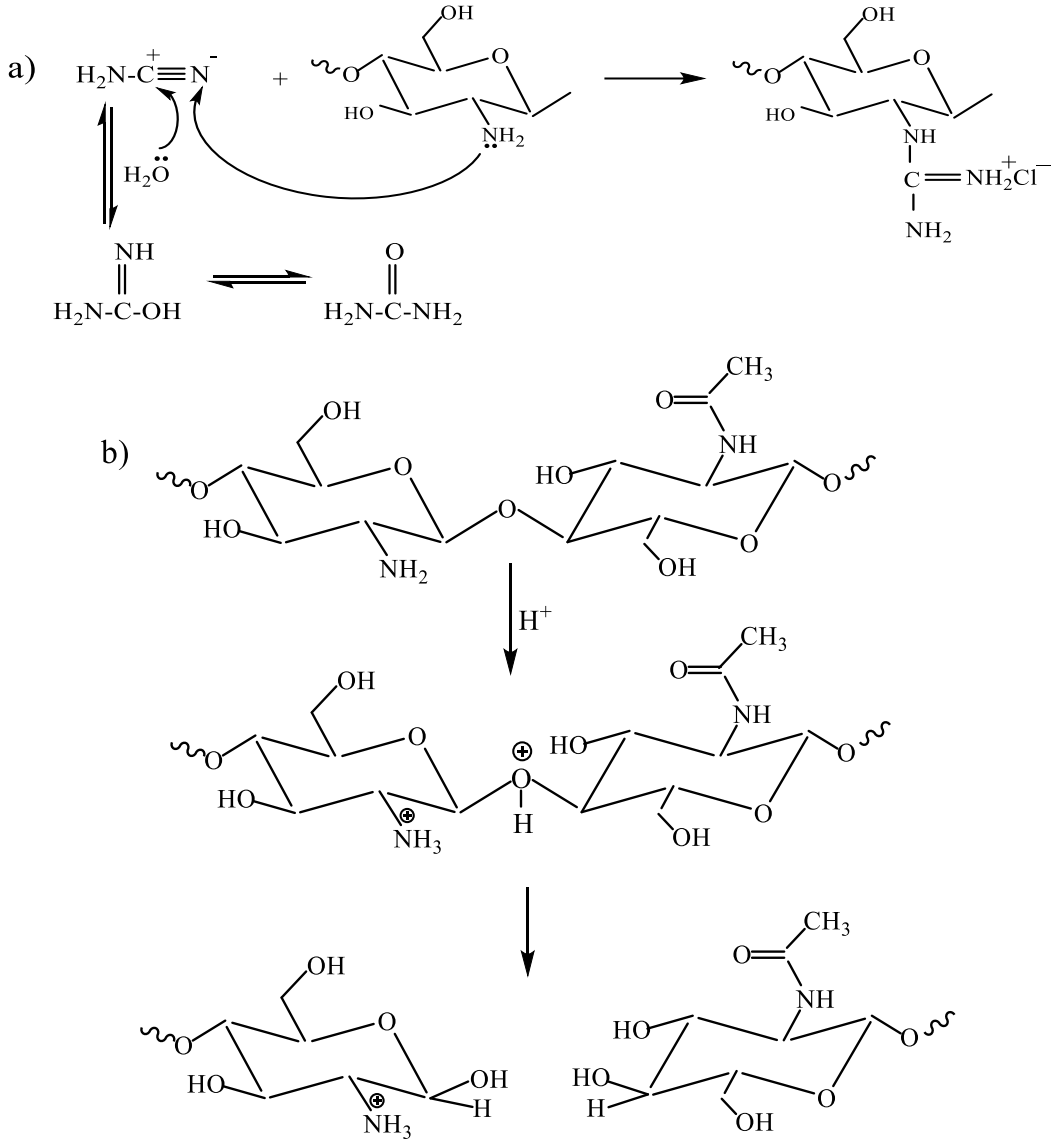


**Figure 1** Formation of side effects during guanidation of chitosan using cyanamide in the presence of acid solutions.

In our previous studies, we demonstrated that the introduction of guanidine groups into polysaccharide structures results in the formation of bioactive derivatives exhibiting pronounced antimicrobial activity [21,22]. A clear correlation was established between the structural features of the modified compounds and their pharmacological properties, highlighting the potential of this approach for the targeted synthesis of guanidine-containing polysaccharide derivatives with tunable biological functions.

Considering the adverse effects of acidic solvents on the guanidinylation of chitosan, we propose a modified chemical approach utilizing acetonitrile as the reaction medium. The rationale behind employing an aprotic solvent lies in the suppression of undesired side reactions and the production of *N*-guanidinium chitosan derivatives capable of dissolving over a broad pH range. Guanidinylation of chitosan in acetonitrile effectively prevents hydrolytic degradation of the macromolecular backbone, thereby enabling the synthesis of derivatives with higher molecular weights. A series of *N*-

guanidinium chitosan derivatives with varying degrees of guanidinylation were synthesized by altering the feed ratio of the starting materials (chitosan:cyanamide). The physicochemical properties of the resulting derivatives were thoroughly characterized using FTIR, NMR, XRD, SEM, and DLS techniques. The wound healing and hemostatic efficacy of the synthesized derivatives were evaluated *in vivo*. Our results demonstrate that the introduction of guanidinium groups into the chitosan backbone significantly enhances both wound healing and hemostatic performance compared to the unmodified polysaccharide.

## Materials and methods

### Materials

Chitosan (DD = 85% and $M_W$ = $2.318\times10^5$), cyanamide, acetonitrile was obtained from Sigma-Aldrich. All other chemicals were of analytical grade and used without further purification. All aqueous solutions were prepared using deionized water.

### Synthesis *N*-guanidinium chitosan

Chitosan 1 g was dispersed in 100 mL of acetonitrile and stirred for 2 h. After swelling, cyanamide was added at a molar ratio of chitosan:cyanamide = 1:1 - 4. The reaction mixture was stirred for 10 h at 80 °C, after which the resulting precipitate was separated by decantation, dissolved in 1% hydrochloric acid solution, and re-precipitated with acetone. The obtained precipitate was then dissolved in water and purified by dialysis for 48 h, with 5 changes of dialysis water. Finally, the dialysate was freeze-dried. The degree of substitution (DS) guanidinium derivatives was calculated according to the C/N wt% from the elemental analysis [23].

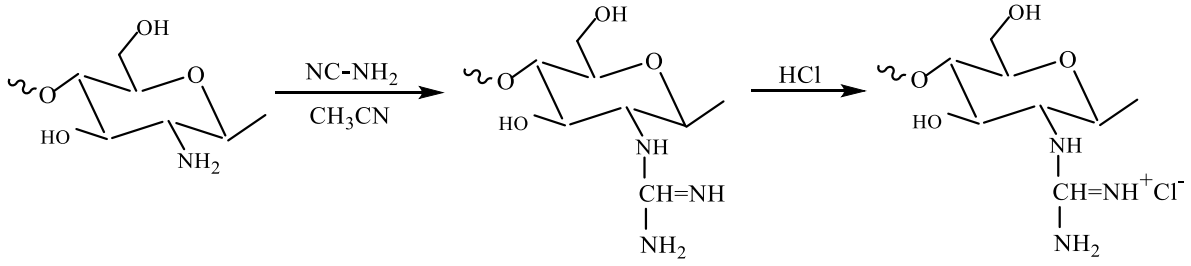


**Figure 2** The synthetic route of *N*-guanidinium chitosan.

### Characterization methods

FTIR spectra of Chitosan and *N*-guanidinium chitosan were recorded in the range from 400 to 4,000 $cm^{-1}$ using Vector-22 Tensor-27 spectrometer (Bruker, Germany). Data collection was performed with a 4 $cm^{-1}$ spectral resolution and 32 scans.

X-Ray diffractograms of the investigated samples were obtained using an X-ray powder diffractometer XRD-6100 (Shimadzu, Japan) with Ni-filter and CuKα radiation source at an accelerating voltage/current of 50 kV/40 mA. The relative intensity was recorded in the scattering range 2θ, varying from 3° to 80° at scanning rate 2° $min^{-1}$. Surface analysis of chitosan and *N*-guanidinium chitosan was performed using a scanning electron microscope (SEM), EVO MA10 (Zeiss, Germany).

The elemental composition of chitosan and the synthesized *N*-guanidinium chitosan samples was determined using a Eura EA elemental analyzer (Italy).

The ζ-potential and hydrodynamic size of chitosan and *N*-guanidinium chitosan samples were determined by dynamic light scattering (DLS) using a Zetasizer Nano-ZS analyzer (Malvern Instruments, UK) at 25 ± 1 °C.

The pKα values of the final reaction products were determined as follows: 50 mg of the sample was dissolved in water, and the resulting solution was acidified to pH 3 using 0.1 N HCl. Subsequently, the solution was titrated under constant stirring by the incremental addition of 0.1 N NaOH. The pH was continuously monitored using a SevenCompact S220-Basic pH meter (Mettler Toledo, Germany). The pKα was determined as the pH value corresponding to the

midpoint of the plateau on the titration curve, as described in reference [24].

The molecular weight of the samples was determined by gel permeation chromatography. The analyses were performed using an Agilent 1260 Infinity II chromatographic system equipped with the following components: An Agilent 1260 Infinity II Iso Pump (G7110B) (Agilent Technologies, GmbH, Germany); Suprema Lux 1,000 Å (8×300 mm, 5 μm) and Suprema Linear S (8×300 mm, 5 μm) columns (PSS Polymer Standards Service GmbH, Germany); a G7800A 1260 GPC/SEC MDS detector; a UV-VIS detector (G7115A 1260 DAD WR); a refractive index detector (1260 Infinity II RI); and a dual-angle light scattering detector (1260 Infinity II Dual Angle LS). The intrinsic viscosity of the samples was determined using an Ubbelohde viscometer (capillary diameter = 0.34 mm) in an acetate buffer solution at 25 °C.

The solubility of chitosan and *N*-guanidinium chitosan samples at different pH values was determined by turbidimetric titration. Chitosan and *N*-guanidinium chitosan were dissolved in 5 mL of 1% hydrochloric acid, followed by the addition of 5% sodium hydroxide solution. Optical density was measured at 600 nm using a UV 1280 spectrophotometer (Shimadzu, Japan).

**Evaluation of the wound healing effect of *N*-guanidinium chitosan**

The animal experiments were approved by the Ethics Committee of the Institute of Bioorganic Chemistry of the Academy of Sciences of Uzbekistan and conducted in accordance with the European Convention for the Protection of Vertebrate Animals used for Experimental and Other Scientific Purposes [25]. The experimental animal groups were distributed as follows: 1st group - control group, without treatment; 2nd group - treated with 0.5% Chitosan solution; 3rd group - treated with 0.5% *N*-guanidinium chitosan (DS = 0.16); 4th group - treated with 0.5% *N*-guanidinium chitosan (DS = 0.45).

For wound formation, rats were anaesthetized by intraperitoneal injection of sodium ethaminal (50 mg/kg). The dorsal region was then depilated and, after antiseptic treatment, a 2.5 $cm^2$ area of skin was excised along the underlying fascia [26]. After one day, the treatment was carried out. The wounds were treated with aqueous solutions (100 μL), daily during the entire treatment period.

The wounds were left uncovered. Throughout the entire study period, control studies were carried out, which took into account the following parameters of the course of the wound process: the presence and nature of the inflammatory reaction, the condition of the edges and the bottom of the wound, the timing of the wound cleansing from necrotic tissue, the timing of the onset of wound epithelization. To assess the healing process, wound diameter was measured with a caliper. The area of induced wounds was recorded by digital Vernier caliper (HD-5214) on days 3, 6, 9 and 12 of treatment, and the wound healing rate was calculated using the following equation [27]:

$$Wound\ healing\ rate = \frac{S_0 - S}{S_0} \cdot 100\%$$

where $S_0$ is the area of the initial wound ($cm^2$) and $S$ is the area of the wound after the reproduced pathology ($cm^2$).

The obtained results were presented as mean ± standard deviation. The statistical analysis of the data was performed using the 1-way analysis of variance (ANOVA) with a significant level of $p = 0.05$. The value of $p < 0.05$ was considered to be statistically significant.

**Rat liver injury models**

The animal experiments were approved by the Ethics Committee of the Institute of Bioorganic Chemistry of the Academy of Sciences of Uzbekistan and conducted in accordance with the European Convention for the Protection of Vertebrate Animals used for Experimental and Other Scientific Purposes [25]. Experimental animals were rats with a body weight ranging from 200 - 220 g. Animals were kept under standard laboratory conditions in a vivarium maintained at 22 ± 3 °C, with ad libitum access to food and water. They were randomly allocated into 10 groups: 1st group - control group, without treatment; 2nd group - treated with 0.25% Chitosan solution; 3rd group - treated with 0.5% Chitosan solution; 4th group - treated with 1.0% Chitosan solution; 5th group - treated with 0.25% *N*-guanidinium chitosan (DS = 0.16) solution; 6th group - treated with 0.5% *N*-guanidinium chitosan (DS = 0.16)

solution; 7th group - treated with 1.0% *N*-guanidinium chitosan (DS=0.16) solution; 8th group - treated with 0.25% *N*-guanidinium chitosan (DS n = 0.45) solution; 9th group - treated with 0.5% *N*-guanidinium chitosan (DS = 0.45) solution; 10th group - treated with 1.0% *N*-guanidinium chitosan (DS = 0.45) solution.

For wound formation, rats were anaesthetized by intraperitoneal injection of sodium ethaminal (50 mg/kg). The animals were secured in the prone position on the operating table. A midline laparotomy was performed along the inferior edge of the rat's costal arch to provide adequate access to the left liver lobe. The liver apex was then transected to create an open wound approximately 1.0 cm in length, followed by free bleeding. Subsequently, 50 μL of the tested sample solutions at concentrations of 0.25%, 0.5%, and 1.0% were applied. The bleeding time was recorded by stop-watch.

**Results and discussion**

The degree of chitosan guanidination, calculated based on elemental analysis data using the carbon-to-nitrogen ratio (**Table 1**), confirms the presence of nitrogen-rich guanidinium groups in the product. A decrease in the C/N ratio indicates successful incorporation of nitrogen-containing guanidine moieties into the chitosan backbone. Based on the calculated C/N values, the degree of guanidination at chitosan-to-cyanamide molar ratios ranging from 1:1 to 1:4 varies from 0.16 to 0.45. These results demonstrate that increasing the amount of cyanamide in the reaction system leads to a deeper modification of chitosan. As the degree of guanidination increases, the pKα of the resulting samples rises from 7.7 to 8.3, indicating enhanced basicity of the functional groups due to the incorporation of guanidine fragments. Changes in the surface charge of the synthesized *N*-guanidinium chitosan samples suggest the presence of chloride anions in their structure, which compensate for the positive charge of the guanidinium groups. Moreover, with an increasing degree of substitution, the content of $Cl^-$ ions also increases, resulting in a reduction of the overall positive charge of the macromolecular backbone.

**Table 1** Characteristics of the synthesized compounds at different chitosan/cyanamide molar ratios.

| Molar ratios | C | N | C/N | DS | ζ-potential, mV | pKα | $M_w \times 10^5$ | η, g/dl |
|---|---|---|---|---|---|---|---|---|
| Chitosan | 36.7 | 6.6 | 5.56 | - | 38 | 6.5 | 2.318 | 4,56 |
| 1:1 | 32.5 | 8.0 | 4.06 | 0.16 | 50 | 7.7 | 2.335 | 4,43 |
| 1:2 | 33.0 | 9.2 | 3.58 | 0.27 | 46 | 8.0 | 2.346 | 4,31 |
| 1:3 | 33.5 | 11.0 | 3.04 | 0.38 | 41 | 8.1 | 2.352 | 4,23 |
| 1:4 | 33.6 | 11.3 | 2.97 | 0.45 | 35 | 8.3 | 2.357 | 4,10 |

An increase in the guanidino group content within the chitosan structure results in a corresponding rise in the molecular weight of the synthesized derivatives. These findings provide compelling evidence that the guanidination of chitosan in an acetonitrile medium does not lead to destructive modifications. At the same time, an increase in the degree of substitution in *N*-guanidinylated chitosan derivatives is accompanied by a decrease in solution viscosity, which is presumably due to enhanced electrostatic repulsion between polymer backbone, thereby preventing their aggregation. Further evidence of the inhibitory effect of the guanidinium groups present on particle aggregation is provided by the data shown in **Figure 3**.

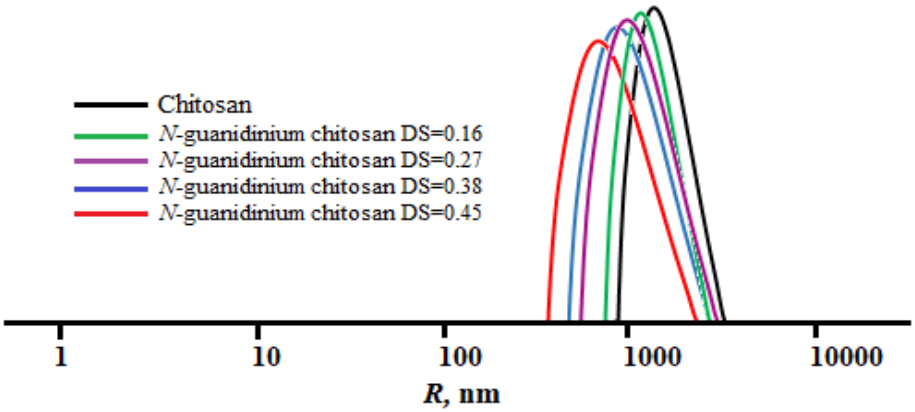


**Figure 3** Distribution of chitosan and *N*-guanidinium chitosan particles by hydrodynamic radius.

The **Figure 3** shows the particle size distribution by hydrodynamic radius (*R*, nm) for the native chitosan and its synthesized *N*-guanidinium chitosan derivatives. Analysis of the obtained curves enables the evaluation of the effect of the DS on the size characteristics of the samples in solution. The hydrodynamic diameter of unmodified chitosan ranges from approximately 900 to 5,800 nm and exhibits a unimodal numerical distribution pattern. For the derivative with DS = 0.16, the distribution remains close to that of the unmodified polymer, whereas a notable shift toward smaller radii is observed for samples with DS = 0.27 and 0.38. The most pronounced reduction in particle size is recorded for the derivative with DS = 0.45, for which the main peak of the distribution lies within the range of 650 - 4,100 nm. The presented data suggest that an increase in the DS of the synthesized chitosan derivatives leads to a more compact organization of the particles.

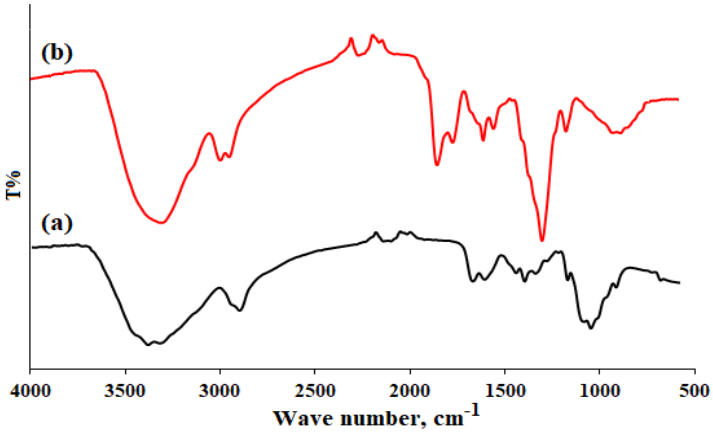


**Figure 4** FTIR spectra of chitosan (a), *N*-guanidinium-chitosan with DS = 0.45 (b).

Chitosan displayed characteristic bands at 1,643 and 1,556 $cm^{-1}$ which are related to amide I & II, respectively, 1,082 $cm^{-1}$ (C-O stretching), 2,945 - 2,864 $cm^{-1}$ (-CH stretching), 1,376 $cm^{-1}$ (-$CH_3$ stretching) and at 3,448 $cm^{-1}$ (-$NH_2$ and -OH stretching). For *N*-guanidinium chitosan, new bands appeared at 1,664, 1,570 and 1,258 $cm^{-1}$ owing to stretching of C=N, C=$NH_2^+$ and C-N of the guanidinyl group, respectively (**Figure 4**).

The solid-state $^{13}C$ NMR spectral data are shown in **Figure 5**. The *N*-guanidinium chitosan sample displays characteristic signals in the chemical shift range of 23 - 106 ppm, corresponding to the anhydroglucose units, similar to those observed in unmodified chitosan, confirming the preservation of the polysaccharide backbone. In contrast to native chitosan, the spectrum of the synthesized *N*-guanidinium derivative exhibits a distinct signal at 161 ppm, which provides evidence for the successful introduction of guanidinium groups.

Additionally, a peak observed at 178 ppm can be attributed to the acetate fragment, which is commonly present in chitosan-based materials.

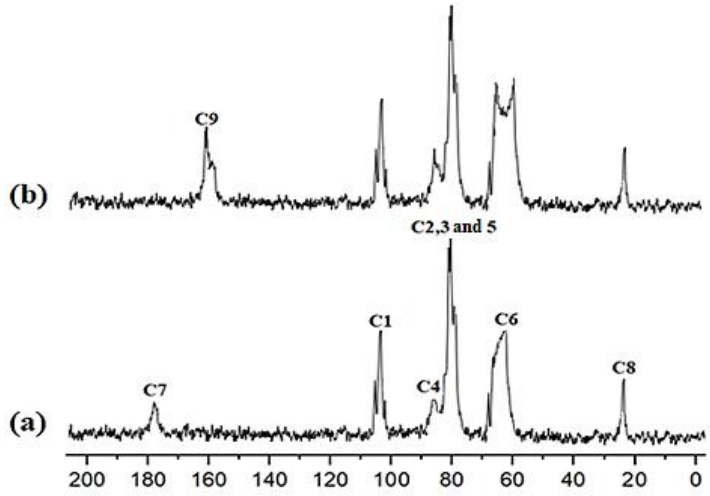


**Figure 5** $^{13}$C NMR of chitosan (a) and *N*-guanidinium chitosan with DS = 0.45 (b).

The obtained SEM results enabled visualization of the surface morphological features of chitosan (**Figure 6**). The SEM image of chitosan reveals a plate-like structure with characteristic cracks and fractures, which may indicate the brittleness of the material after drying. The surface appears relatively smooth, with occasional defects and microcracks, suggesting a possible oriented arrangement of macromolecules. The presence of sharp edges and brittle fractures may be indicative of crystalline regions within the chitosan matrix. In contrast, the SEM image of *N*-guanidinium chitosan exhibits a loose, disordered structure with pronounced layering and a lack of well-defined edges, which suggests the occurrence of biopolymer amorphization during modification.

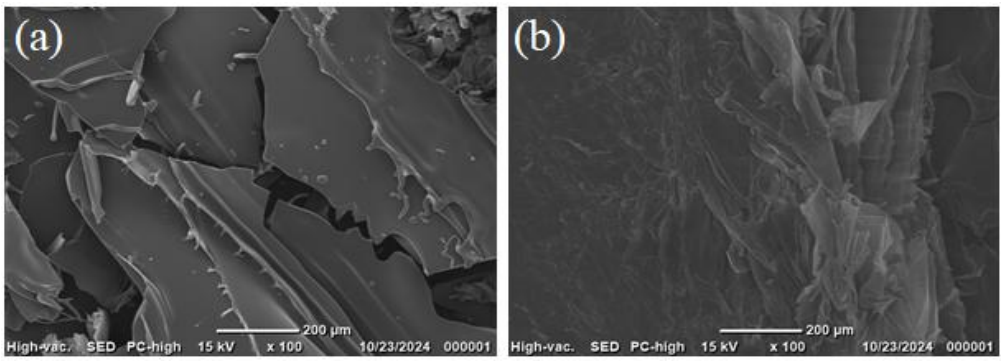


**Figure 6** SEM of chitosan (a) and *N*-guanidinium chitosan with DS = 0.45 (b).

**Figure 7** shows the results of a comparative XRD analysis of chitosan and *N*-guanidinium chitosan. The presented diffractogram shows a broad, low-intensity peak around 20° (2θ), which indicates the low crystallinity of the native chitosan [28]. In addition, weak diffraction peaks at 14° and 26° (2θ) are observed, which can be attributed to residual ordered domains within the polymer structure. Following chemical modification, a further decrease in peak intensity and an increase in the amorphous halo are observed, suggesting disruption of crystalline domains and an overall increase in the amorphous nature of the chitosan. This can be attributed to the reduction of intra- and intermolecular hydrogen bonding, as well as alterations in the packing

of the chitosan polymer chains as a result of chemical modification. The obtained data confirm that the introduction of guanidinium groups contributes to the breakdown of residual crystalline regions in the chitosan matrix. Thus, the XRD analysis clearly demonstrates significant structural changes in chitosan upon chemical modification.

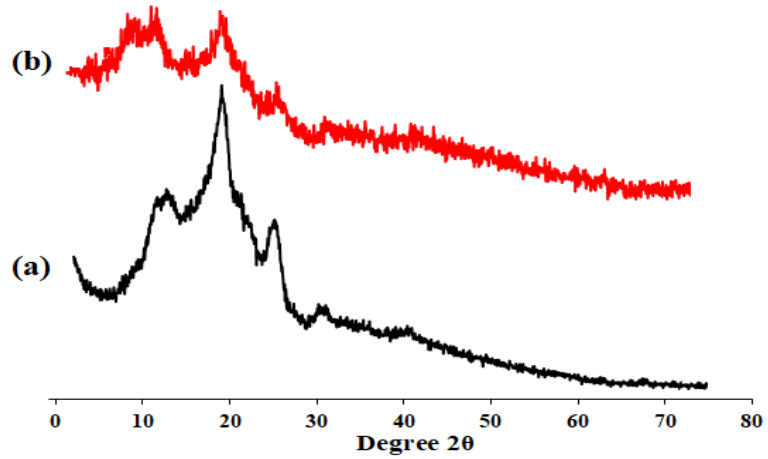


**Figure 7** XRD chitosan (a) and *N*-guanidinium DS = 0.45 (b).

The dependence of chitosan and *N*-guanidinium chitosan sample solubility on pH was investigated as a function of the DS. **Figure 8** shows the variation in optical density (absorbance) of chitosan and its derivatives with different DS values as a function of pH. As shown in the graph, native chitosan exhibits the highest absorbance values, which increase with rising pH, reaching a maximum at pH 9. This trend is associated with a gradual decrease in chitosan solubility as the pH increases from 3 to 9, leading to the formation of insoluble particles and a corresponding rise in optical density. In contrast, *N*-guanidinium chitosan samples with DS = 0.16 and 0.45 show significantly lower absorbance values across the entire pH range. The sample with a higher degree of substitution demonstrates especially low absorbance, which may indicate enhanced solubility and improved solution stability due to the presence of a greater number of guanidinium groups. This also suggests an increase in the hydrophilicity of the modified chitosan.

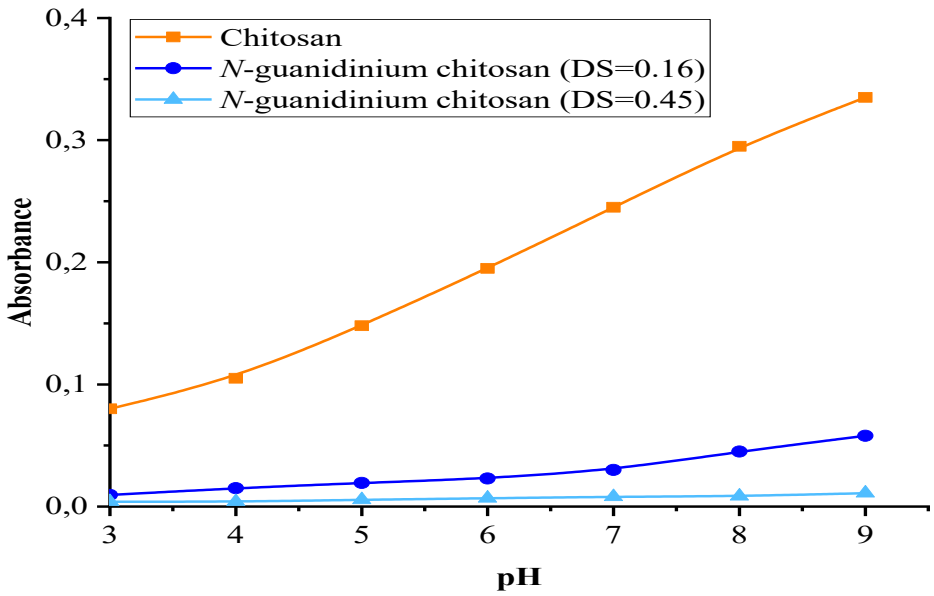


**Figure 8** Dependence of solubility of chitosan and *N*-guanidinium chitosan derivatives on the pH of the medium.

Guanidine is a structural fragment of the amino acid arginine, which is known to act as a nitric oxide donor for vascular endothelial cells [29]. As a result, arginine exhibits a wide range of therapeutic effects, including the stimulation of wound healing [30-32]. The synthesized *N*-guanidinium chitosan derivatives contain guanidine moieties within their structure, which may similarly contribute to enhanced wound healing. Therefore, it can be hypothesized that these derivatives are capable of activating wound-healing mechanisms analogous to those induced by arginine. To support this hypothesis, we investigated the wound-healing properties of *N*-guanidinium chitosan solutions with varying degrees of substitution (**Figure 9** and **10**).

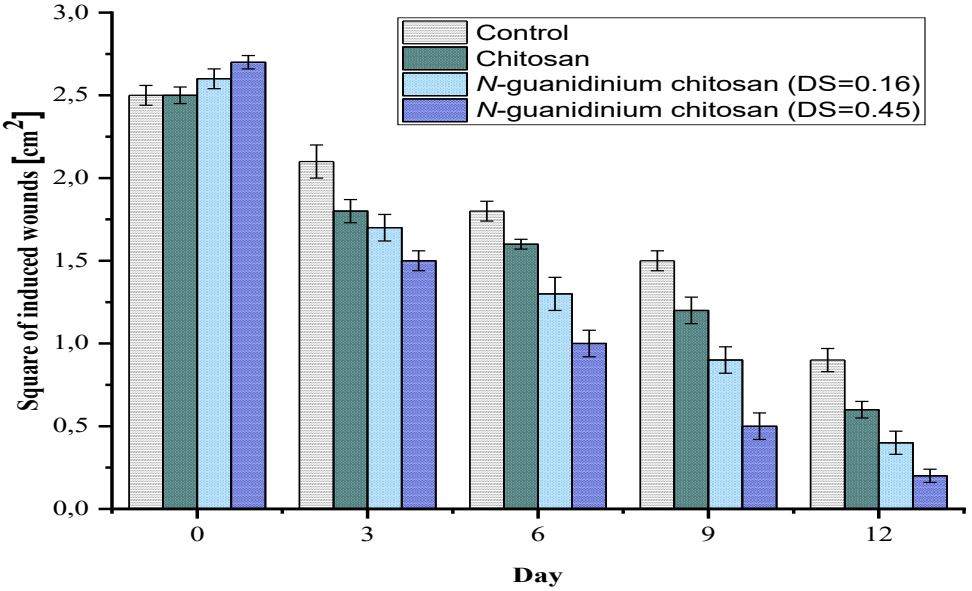


**Figure 9** Comparative wound healing properties of chitosan and synthesized *N*-guanidinium chitosan derivatives.

In the pharmacological studies, a reproducible skin wound model was established, with wound areas ranging from 2.50 ± 0.06 to 2.70 ± 0.09 $cm^2$. Macroscopically after damage was inflicted for 15 - 30 min, changes in the form of accumulation of intercellular fluid and slightly pronounced capillary fullness were noted in the edges of the induced wounds; the edges were also slightly swollen and raised above the surface. The absence of purulent infiltration and pronounced hyperemia confirms the reliability and consistency of the experimental model.

In the control group, the progression of regenerative processes was significantly slower compared to the groups treated with 0.5% solutions of chitosan and the synthesized *N*-guanidinium chitosan derivatives (**Figure 9**). Thus, on the $3^{rd}$, $6^{th}$, $9^{th}$ and $12^{th}$ days the wound area was 2.1 ± 0.13, 1.80 ± 0.08, 1.50 ± 0.08, and 0.90 ± 0.06 $cm^2$, and the calculated healing rate was 16, 28, 40 and 64 %, respectively. These results reflect a typical and sequential progression through the phases of wound healing, consistent with the normal reparative response following injury.

In contrast to the control group, the application of a 0.5% chitosan solution significantly accelerated wound healing (**Figure 9**). In the treated group, the wound areas on was $3^{rd}$, $6^{th}$, $9^{th}$, and $12^{th}$ were 1.8 ± 0.07, 1.6 ± 0.03, 1.2 ± 0.08, and 0.6 ± 0.05 $cm^2$, respectively, with corresponding healing rates of 28%, 36%, 52%, and 76%. Moreover, the phases of the reparative process including wound edge and bed condition, necrotic tissue clearance, scab formation, and subsequent epithelialization progressed more rapidly in this group compared to the control, indicating enhanced therapeutic efficacy of chitosan treatment.

More effective wound healing was observed with the application of 0.5% solutions of the synthesized *N*-guanidinium chitosan samples. When wounds were treated with a 0.5% solution of *N*-guanidinium chitosan with a degree of substitution of 0.16, the wound areas on days $3^{rd}$, $6^{th}$, $9^{th}$, and $12^{th}$ were 1.7 ± 0.08, 1.3 ± 0.1, 0.9 ± 0.08, and 0.4 ± 0.07 $cm^2$ respectively,

corresponding to healing rates of 36%, 48%, 65%, and 85%. These findings demonstrate that the presence of guanidinium groups in the chitosan structure contributes to a significant acceleration of wound healing compared to both the control group and the group treated with a 0.5% chitosan solution.

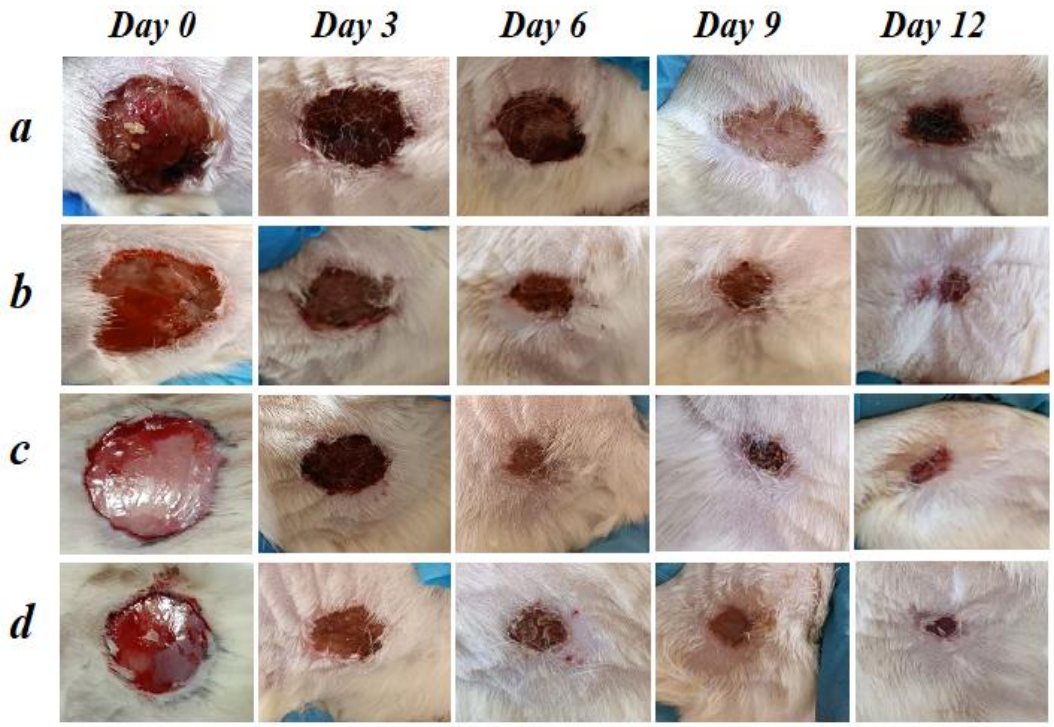


**Figure 10** Wound healing process in different groups of rats: a - control group, without treatment; b - treated with 0.5 % Chitosan solution; c - treated with 0.5% *N*-guanidinium chitosan (DS = 0.16) solution; d - treated with 0.5% *N*-guanidinium chitosan (DS = 0.45) solution.

The most pronounced wound-healing activity was observed with the application of a 0.5% solution of *N*-guanidinium chitosan with a degree of substitution of 0.45 (**Figure 10(d)**). Thus, on the 3$^{rd}$, 6$^{th}$, 9$^{th}$, and 12$^{th}$ days the wound area was $1.5 \pm 0.06$, $1.0 \pm 0.08$, $0.5 \pm 0.08$, and $0.2 \pm 0.04$ cm$^2$, and the calculated healing rate was 44, 63, 81 and 93%, respectively. Dynamic monitoring of the healing process in this experimental group revealed significantly accelerated wound cleansing, crust formation, and re-epithelialization compared to other groups. Comparative pharmacological assessment showed that while treatment with a 0.5% chitosan solution effectively promoted tissue repair in all animals, the healing outcomes measured by both wound area reduction and closure rate were significantly enhanced in the groups treated with *N*-guanidinium chitosan derivatives at equivalent concentrations.

Thus, all tested samples demonstrated the ability to accelerate the wound healing process; however, the 0.5% solutions of *N*-guanidinium chitosan with a degree of substitution of 0.45 proved to be the most effective (**Figure 10(d)**). These samples exhibited statistically significant superiority over both unmodified chitosan and the *N*-guanidinium chitosan derivative with a substitution degree of 0.16. According to the experimental data, an increase in the guanidinium content within the chitosan structure enhances the reparative process by promoting more rapid wound closure, facilitating the removal of necrotic tissue, supporting crust formation, and accelerating re-epithelialization.

In the case of *N*-guanidinium chitosan, the enhanced wound healing properties compared to native chitosan are presumably attributed to the synergistic interaction of its structural components. Considering the classical mechanisms of the 4 main phases of wound healing [26,33], it can be hypothesized that the incorporation of guanidinium fragments into the chitosan macromolecule contributes to the amplification

of biological activity at various stages of tissue regeneration. As reported in the review by Feng *et al.* [34], chitosan actively participates in the first 3 stages of wound healing. During the hemostasis phase, the amino groups of chitosan promote platelet and erythrocyte aggregation and inhibit fibrinolysis, thereby accelerating the formation of the primary hemostatic plug. In the inflammatory phase, chitosan exhibits pronounced antimicrobial activity, effectively suppressing the growth of pathogenic microorganisms and reducing the risk of wound infection. In the proliferation phase, the depolymerization of chitosan results in the formation of *N*-acetylglucosamine, which in turn stimulates fibroblast proliferation and collagen synthesis, supporting tissue reconstruction. An additional contribution is made by the guanidinium moieties, which are capable of inducing nitric oxide (NO) release a key signaling molecule involved in the regulation of vascular tone, thereby enhancing microcirculation, oxygen delivery, and nutrient transport to the damaged area. This is likely to promote and accelerate reparative processes. Nevertheless, the molecular mechanisms underlying the NO-releasing capacity of guanidinium groups warrant further in-depth investigation. Our experimental data support the significant role of guanidinium functionalities as a potentiating factor in the wound healing process, reinforcing the biological performance of chitosan. Thus, it can be proposed that the synergism between chitosan and guanidinium groups results in a more potent and multifaceted wound healing effect, as confirmed by our preliminary findings.

Some polymeric compounds containing cationic groups in their structure exhibit hemostatic activity through electrostatic interactions with negatively charged blood components [35]. Experimental studies have confirmed that the introduction of additional cationic groups into the chitosan structure enhances its solubility in neutral and alkaline media and improves its hemostatic properties [36]. To broaden the potential biomedical applications of guanidine-containing chitosan derivatives, the hemostatic properties of the synthesized *N*-guanidinium chitosan samples were investigated in the next stage of pharmacological evaluation. The results of these pharmacological studies are presented in **Figure 11**.

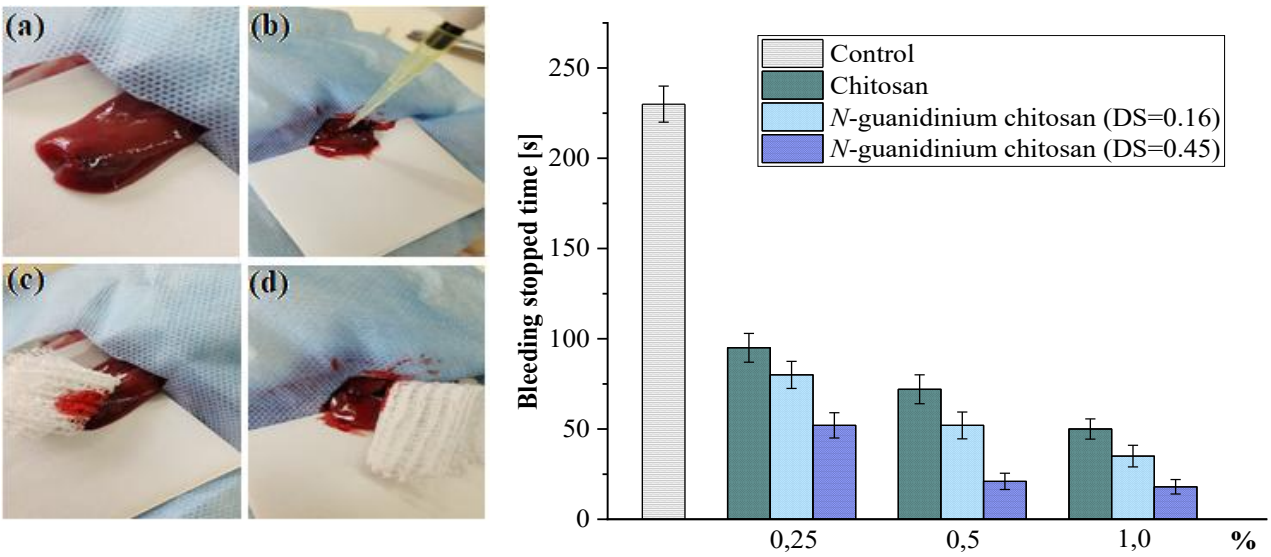


**Figure 11** Hemostasis in rat liver injury: Injured liver (a); application of the test compound solutions (b); hemostatic effect of 0.5% solutions of chitosan (c) and *N*-guanidinium chitosan (d).

Analysis of the presented data indicates that all tested samples reduce bleeding time compared to the control. The difference is particularly pronounced when using 0.25% - 1.0% solutions of chitosan derivatives modified with guanidinium groups. At all investigated concentrations (0.25%, 0.5% and 1.0%), the *N*-guanidinium chitosan samples exhibit significantly higher hemostatic activity than unmodified chitosan, as evidenced by shorter hemostasis times. Specifically, the bleeding times observed for 0.1%, 0.25%, and 0.5%

chitosan solutions were 90 ± 8, 79 ± 7, and 52 ± 6 s, respectively. In contrast, application of *N*-guanidinium chitosan solutions (DS = 0.16 and 0.45) at concentrations of 0.25%, 0.5%, and 1.0% resulted in bleeding times of 78 ± 9 and 55 ± 7, 52 ± 6 and 21 ± 5, 34 ± 8 and 18 ± 6 s, respectively. The enhanced hemostatic performance of *N*-guanidinium chitosan at higher DS may be attributed to more efficient electrostatic interactions with negatively charged blood components.

Chitosan exerts its hemostatic effect through a combined mechanism involving electrostatic interactions, platelet activation, and the formation of a physical barrier. A key role in this process is played by the amine groups in the chitosan backbone, which, under physiological conditions, facilitate strong electrostatic attraction to negatively charged blood cells [37]. Guanidinylation of chitosan represents an effective strategy to enhance the hemostatic performance of polymeric materials by increasing their cationic character. We hypothesize that the introduction of guanidino groups significantly elevates the density of positive charges on the polymer, thereby strengthening interactions with negatively charged components of blood including platelets, erythrocytes, and plasma proteins. This promotes rapid cellular adhesion to the polymer surface, triggers platelet activation, and accelerates clot formation. Unlike primary amines, guanidinium moieties remain protonated under mildly alkaline conditions, ensuring consistent coagulatory activity across a broad range of biological environments, including during active bleeding. In summary, the obtained results suggest that guanidinium functionalization of chitosan is a promising strategy for the development of novel and effective hemostatic agents.

## Conclusions

This study substantiates the feasibility of synthesizing *N*-guanidinium chitosan derivatives with varying degrees of substitution, ζ-potential values, and pKα in an acetonitrile medium. The introduction of guanidine groups into the chitosan structure in the presence of cyanamide in acetonitrile does not lead to hydrolytic degradation of the polymer backbone. An increase in the degree of substitution of the obtained derivatives correlates with an increase in their molecular weight. It was demonstrated that the degree of substitution can be controlled by adjusting the molar ratio of the guanidinating agent to chitosan. The incorporation of guanidine groups into the chitosan macromolecule enhances its solubility in neutral and alkaline media. Pharmacological studies confirmed that the synthesized chitosan derivatives exhibit pronounced wound healing and hemostatic activities. These promising results suggest that guanidine-functionalized chitosan derivatives have potential applications in medicine as novel multifunctional biomaterials.

## Acknowledgements

This study received financial support from the Innovative Development Agency of the Republic of Uzbekistan (Project No. FL-8824063355).

## Declaration of Generative AI in Scientific Writing

The authors disclose that generative tools were employed exclusively for language editing and grammatical improvement during manuscript preparation. These tools did not contribute to the generation of scientific content, data processing, or interpretation. All research findings, analyses, and conclusions are entirely the responsibility of the authors, who have thoroughly reviewed and validated the final manuscript.

## CRediT Author Statement

**O Akhmedov:** Writing - Original draft; Supervision; Formal analysis; Data curation. **J Abdurakhmanov:** Writing - review & editing; Methodology; Conceptualization. **Sh Shomurotov:** Writing - review & editing; Formal analysis. **L You:** Resources; Methodology; Conceptualization. **A Turaev:** Resources; Methodology; Conceptualization. **J Makhkamov:** Investigation; Data Curation; Formal analysis. **O Radjabov:** Investigation; Formal analysis. **A Khusenov:** Investigation; Formal analysis.

## References

[1] MK Yazdi, F Seidi, A Hejna, P Zarrintaj, N Rabiee, J Kucinska-Lipka, MR Saeb and SA Bencherif. Tailor-made polysaccharides for biomedical applications. *ACS Applied Bio Materials* 2024; **7(7)**, 4193-4230.

[2] ZU Arif. The role of polysaccharide-based biodegradable soft polymers in the healthcare sector. *Advanced Industrial and Engineering Polymer Research* 2025; **8(1)**, 132-156.

[3] Q Meng, Y Sun, H Cong, H Hu and FJ Xu. An overview of chitosan and its application in infectious diseases. *Drug Delivery and Translational Research* 2021; **11**, 1340-1351.

[4] H Yadav, R Malviya and N Kaushik. Chitosan in biomedicine: A comprehensive review of recent developments. *Carbohydrate Polymer Technologies and Applications* 2024; **8**, 100551.

[5] A Sidarenka, A Kraskouski, V Savich, O Akhmedov, V Nikalaichuk, A Herasimovich, K Hileuskaya and V Kulikouskaya. Design of sponge-like chitosan wound dressing with immobilized bacteriophages for promoting healing of bacterially infected wounds. *Journal of Polymers and the Environment* 2024; **32**, 3893-3909.

[6] F Fitriagustiani, AZ Mustopa, S Budiarti, MF Warsito, RD Pratiwi, DF Agustiyanti and M Nurfatwa. Formulation and characterization of alginate coated chitosan nanoparticles as therapeutic protein for oral delivery system. *Trends in Sciences* 2022; **19(18)**, 5797.

[7] L Chen, Y Xie, X Chen, H Li, Y Lu, H Yu and D Zheng. O-carboxymethyl chitosan in biomedicine: A review. *International Journal of Biological Macromolecules* 2024; **275(2)**, 133465

[8] MES Miranda, C Marcolla, CA Rodrígues, HM Wilhelm, MR Sierakowski, TMB Bresolin and RA de Freitas. Chitosan and N-carboxymethylchitosan: I. The role of N-carboxymethylation of chitosan in the thermal stability and dynamic mechanical properties of its films. *Polymer International* 2006; **55**, 961-969.

[9] S Kalliola, E Repo, V Srivastava, F Zhao, JP Heiskanen, JA Sirviö, H Liimatainen and M Sillanpää. Carboxymethyl chitosan and its hydrophobically modified derivative as pH-switchable emulsifiers. *Langmuir* 2018; **34**, 2800-2806.

[10] C Ardean, NS Nemeş, A Negrea, M Ciopec, N Duteanu, P Negrea, M Ciopec, N Duteanu, P Negrea, D Duda-Seiman and V Musta. Factors influencing the antibacterial activity of chitosan and chitosan modified by functionalization. *International Journal of Molecular Sciences* 2021; **22(14)**, 7449.

[11] H Tan, R Ma, C Lin, Z Liu and T Tang. Quaternized chitosan as an antimicrobial agent: antimicrobial activity, mechanism of action and biomedical applications in orthopedics. *International Journal of Molecular Sciences* 2013; **14(1)**, 1854-1869.

[12] W Sajomsang, P Gonil and S Tantayanon. Antibacterial activity of quaternary ammonium chitosan containing mono or disaccharide moieties: Preparation and characterization. *International Journal of Biological Macromolecules* 2009; **44(5)**, 419-427.

[13] T Ishikawa. Guanidine chemistry. *Chemical and Pharmaceutical Bulletin* 2010; **58(12)**, 1555-1564.

[14] P Pham, S Oliver and C Boyer. Design of antimicrobial polymers. *Macromolecular Chemistry and Physics* 2023; **224(3)**, 2200226.

[15] J Zhang, L Hu, Q Zhang, C Guo, C Wu, Y Shi, R Shu and L Tan. Polyhexamethylene guanidine hydrochloride modified sodium alginate nonwoven with potent antibacterial and hemostatic properties for infected full-thickness wound healing. *International Journal of Biological Macromolecules* 2022; **209**, 2142-2150.

[16] AR Gomes, CL Varela, AS Pires, EJ Tavares-da-Silva and FMF Roleira. Synthetic and natural guanidine derivatives as antitumor and antimicrobial agents: A review. *Bioorganic Chemistry* 2023; **138**, 106600.

[17] FV Drozdov and VM Kotov. Guanidine: A simple molecule with great potential: From catalysts to biocides and molecular glues. *INEOS Open* 2020; **3**, 200-213.

[18] OR Akhmedov, SA Shomurotov and AS Turaev. Comparative studies of the chemical interaction of guanidine with dialdehyde cellulose and pectin. *Russian Journal of Bioorganic Chemistry* 2023; **49(7)**, 1587-1595

[19] HE Salama, GR Saad and MW Sabaa. Synthesis, characterization, and biological activity of cross-linked chitosan biguanidine loaded with silver nanoparticles. *Journal of Biomaterials Science, Polymer Edition* 2016; **27(18)**, 1880-1898.

[20] A Salama and P Hesemann. New N-guanidinium chitosan/silica ionic microhybrids as efficient adsorbent for dye removal from waste water. *International Journal of Biological Macromolecules* 2018; **111**, 762-768

[21] OR Akhmedov, SA Shomurotov, AS Turaev and AV Sidarenka. Dependence of antimicrobial effects of guanidine-containing pectin derivatives from some structural characteristics. *Drug Development and Registration* 2022; **11(2)**, 38-45.

[22] OR Akhmedov, SA Shomurotov and AS Turaev. Features of synthesis and antimicrobial properties of guanidine-containing carboxymethylcellulose derivatives. *Russian Journal of Bioorganic Chemistry* 2022; **48**, 1379-1386.

[23] X Zhao, JX He and YZ Zhan. Synthesis and characterization of chitosan biguanidine hydrochloride under microwave irradiation. *Polymer Journal* 2009; **41**, 1030-1035.

[24] LAB Rawlinson, SM Ryan, G Mantovani, JA Syrett, DM Haddleton and DJ Brayden. Antibacterial effects of poly(2-(dimethylamino ethyl)methacrylate) against selected gram-positive and gram-negative bacteria. *Biomacromolecules* 2010; **11(2)**, 443-453.

[25] C de l'Europe. European Convention for the protection of vertebrate animals used for experimental and other scientific purposes. *Official Journal* 1986; **L222**, 37-87.

[26] K Khainskaya, K Hileuskaya, V Nikalaichuk, A Ladutska, O Akhmedov, N Abrekova, L You, P Shao and M Odonchimeg. Chitosan-gallic acid conjugate with enhanced functional properties and synergistic wound healing effect. *Carbohydrate Research* 2025; **553**, 109496.

[27] Y Li, Q Leng, X Pang, H Shi, Y Liu, S Xiao, L Zhao, P Zhou and S Fu. Therapeutic effects of EGF-modified curcumin/chitosan nano-spray on wound healing. *Regenerative Biomaterials* 2021; **8(2)**, 1-9.

[28] J Kumirska, M Czerwicka, Z Kaczyński, A Bychowska, K Brzozowski, J Thöming and P Stepnowski. Application of spectroscopic methods for structural analysis of chitin and chitosan. *Marine Drugs* 2010; **8**, 1567-1636.

[29] MS Joshi, TB Ferguson, FK Johnson and JR Lancaster. Receptor-mediated activation of nitric oxide synthesis by arginine in endothelial cells. *Proceedings of the National Academy of Sciences* 2007; **104(24)**, 9982-9987.

[30] Y Zhou, G Liu, H Huang and J Wu. Advances and impact of arginine-based materials in wound healing. *Journal of Materials Chemistry B* 2021; **9**, 6738-6750.

[31] MB Witte and A Barbul. Arginine physiology and its implication for wound healing. *Wound Repair and Regeneration* 2003; **11(6)**, 419-423.

[32] HP Shi, D Most, DT Efron, MB Witte and A Barbul. Supplemental L-arginine enhances wound healing in diabetic rats. *Wound Repair and Regeneration* 2003; **11(3)**, 198-203.

[33] DJ Yang, SH Moh, DH Son, S You, AW Kinyua, CM Ko, M Song, J Yeo, YH Choi and KW Kim. Gallic acid promotes wound healing in normal and hyperglucidic conditions. *Molecules* 2016; **21(7)**, 899.

[34] P Feng, Y Luo, C Ke, H Qiu, W Wang, Y Zhu, R Hou, L Xu and S Wu. Chitosan-based functional materials for skin wound repair: Mechanisms and applications. *Frontiers in Bioengineering and Biotechnology* 2021; **9**, 650598.

[35] Y Fang, Y Lin, L Wang, Y Weng, Q Chen and H Liu. Clotting blood into an adhesive gel by hemostatic powder based on cationic/anionic polysaccharides and laponite. *Biomacromolecules* 2024; **25(6)**, 3335-3344.

[36] K Kaminski, K Szczubiałka, K Zazakowny, R Lach and M Nowakowska. Chitosan derivatives as novel potential heparin reversal agents. *Journal of Medicinal Chemistry* 2010; **53(10)**, 4141-4147.

[37] KY Chen, TH Lin, CY Yang, YW Kuo and U Lei. Mechanics for the adhesion and aggregation of red blood cells on chitosan. *Journal of Mechanics* 2018; **34(5)**, 725-732.